Calculation of the Fermi velocities of electrons in Sb and Bi

Yu. A. Pospelov, G. S. Grachev, and S. G. Novikov

Sergo Ordzhonikidze Moscow Institute of Control
(Submitted 27 April 1984)
Zh.Eksp. Teor. Fiz. **87**, 2104–2113 (December 1984)

Detailed calculation of the electron Fermi velocities in Sb and Bi is carried out for the first time. The simultaneous (and independent) calculations of the contours of Fermi surface sections and of the velocities v_F on them allow us to obtain pictures of the "hedgehogs" or contours with Fermi-velocity halos. Effective calculation techniques for the determination of both the velocity spectrum at the limiting points and the values of the $(\mathbf{v}\cdot\mathbf{H})_{\max}$ distribution are developed. Analytical expressions are obtained for the case of ellipsoidal Fermi surfaces. A comparison with experimental data on the tilt effect has been carried out. It reveals some errors in the experimental data of Beletskiĭ *et al.* [Sov. Phys. JETP **42**, 531 (1975)], which led to an incorrect analysis of tilt-effect experimental results in Sb and Bi.

1. INTRODUCTION

As is well known, for the description of the properties of elementary excitations in metals near the Fermi surface (quasiparticles—electrons and holes), by which most of the electron properties of metals are determined, it is necessary to know the single-particle velocities $\mathbf{v}=\partial E/\partial\mathbf{k}$ in addition to their energies $E(\mathbf{k})$ ($\mathbf{k}$ is the quasimomentum).

In the traditional methods of calculation, it is quite complicated to obtain the value of the Fermi velocity from the calculated dispersion law $E=E(\mathbf{k})$, because of the necessity of differentiation of functions that are determined with some error. The possibility of the independent calculation in addition to $E(\mathbf{k})$, of the nine differential characteristics of the spectrum, of the gradient $\partial E/\partial\mathbf{k}$, and the Hesse matrix $\|\hat{E}\|\equiv\|\partial^2E/\partial k_i\partial kj\|$, at the $\mathbf{k}$ point in the diagonalization of the secular matrix, as pointed out in Ref. 1, opens up a direct path for calculating of the Fermi velocities of the electrons and holes as well as their various distributions.

In this work, we consider finding the velocity distribution at the limiting points of the Fermi surface (*FS*), $v_{\lim}=v_{\lim}(\varphi)$, in the case of rotation of the direction of $\mathbf{H}$ (in the experiments, this is usually the direction of the magnetic field) in a certain plane (φ is the polar angle of the direction of $\mathbf{H}$), and also the corresponding distribution of the values of the maximal projections of the velocity on this direction[1)], $(\mathbf{v}\cdot\mathbf{H})_{\max}=M(\varphi)$.

As is known, these distributions determine directly a number of acousto-electronic phenomena in metals placed in a magnetic field (see, for example, Refs. 2–4).

If a suitable graphical procedure is provided, we can obtain on the alphanumeric printer of a high speed computer a picture of the "hedgehogs"—the contours $\mathscr{L}(E_F)$ of the Fermi surface with mapped (in a certain scale) projections of the velocity on the corresponding plane of the contour $\mathscr{L}(E_F)$ (for electrons—"spines" outwards, for holes, "spines" inwards) or the contour $\mathscr{L}(E_F)$ with a "halo" of calculated velocities.

To make clear the various situations with the Fermi velocities, it is very useful to consider first ellipsoidal Fermi surfaces, in which case we can obtain analytical expressions. Section 2 is devoted to this.

Section 3 is devoted to algorithms for searches (at a given $\mathbf{H}$) of the limiting points of the Fermi surface and the points k_F that are elements of the Fermi surface, at which the projection of v_F on H is maximal, without carrying out global calculations aimed at reconstructing the entire Fermi surface.

In Sec. 4, the corresponding calculations are carried out for Sb and Bi. As a model of the electron spectra we used: for Sb—the pseudopotential model of Falicov and Lin,[5] the adequacy of which for Sb was established in a series of researches (see Refs. 6–8); for Bi—the model of McClure and Choi,[9] which has been successfully applied to the description of the properties of electrons in Bi (see Ref. 10). In this same section, there is a comparison of the calculations with experimental data (basically, we have used the data of Ref. 11, which were obtained in the study of the tilt effect in Sb and Bi.

Section 5 is devoted to a discussion of the results and brief calculations.

2. FORMULAS FOR ELLIPTICAL EQUAL-ENERGY CONTOURS

Let the equation of an equal-energy contour be

$$ak_x^2+bk_y^2=E_0 \tag{1}$$

and let $b>a$, so that the ratio of the semiaxes of the ellipse (1) $\alpha=(b/a)^{1/2}>1$ (in Fig. 1, the case $\alpha=5$ is shown). If we take the center of the ellipse as the pole, then in polar coordinates we have the equation of the ellipse (1) in the form

$$k=E_0^{1/2}/(a\cos^2\varphi+b\sin^2\varphi)^{1/2}. \tag{2}$$

For the velocity distribution along the equal-energy curve (2), we obtain (the polar diagram of the velocities)

$$v(\varphi)=2k(a^2\cos^2\varphi+b^2\sin^2\varphi)^{1/2}=2(E_0)^{1/2}(a^2\cos^2\varphi+b^2\sin^2\varphi)^{1/2}/(a\cos^2\varphi+b\sin^2\varphi)^{1/2}. \tag{3}$$

It is seen that the polar diagram of the velocities (3) differs from an ellipse (in Fig. 1 it is shown by the dashed line). It is elementary to verify that $v(\varphi)$ increases throughout the interval $0<\varphi<\pi/2$; $v_{\min}=v(0)=2(E_0a)^{1/2}$, $v_{\max}=v(\pi/2)=2(E_0b)^{1/2}$ so that the ratio of the semiaxes of the figure

 0038-5646/84/121215-06$04.00

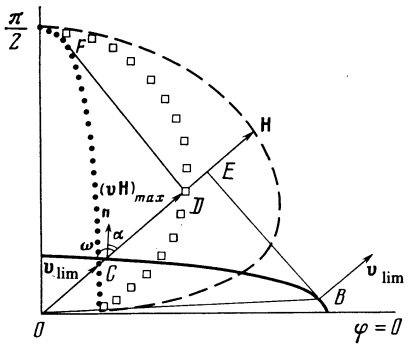

FIG. 1. Velocity characteristics for elliptical section ($\alpha = 5$): solid curve—contour of the section, dashed curve—$v(\varphi)$, squares—$M(\varphi)$, points—$v_{\lim}(\varphi)$.

(3) is, just as in the ellipse (1), equal to α: $v(\pi/2)/v(0) = (b/a)^{1/2} = \alpha$, but the direction of the largest and smallest axes of the figures (1) and (3) are exchanged.

A characteristic feature of the polar diagram $v = v(\varphi)$ are its peculiar "wings," which are more sharply delineated the greater the anisotropy of the ellipse α. The "wings" decrease the anisotropy of the moduli of the velocities on the contour but form a unique "funnel" near the values $\varphi = 0, \pi$. It can be shown that the "wings" appear upon satisfaction of the condition $\alpha > \alpha_{cr}$, where

$$\alpha_{cr}^{(v)} = [(1+\sqrt{5})/2]^{1/2} \approx 1.272. \tag{4}$$

The distribution $v = v(\varphi)$ along the contour should not be confused with the hodograph of the Fermi velocities (for a given contour). It is easy to see that for the ellipse the hodograph of the Fermi velocities will also be an ellipse. The equation of the hodograph $R(\varphi)$ will have the form

$$R(\varphi) = 2(E_0 ab)^{1/2}/(b\cos^2\varphi + a\sin^2\varphi)^{1/2}; \tag{5}$$

the dependence (5) is shown in Fig. 1 by the points. It is obvious that the velocity distribution at the limiting points $v_{\lim}(\varphi)$ is identical with the dependence $R(\varphi)$. A graphical scheme of obtaining the limiting point B is shown in Fig. 1: the straight line $BE \perp \mathbf{H}$ is tangent to the contour $E(\mathbf{k}) = E_0$ at the limiting point B. The end of the vector $\mathbf{v}_{\lim}$, drawn from the pole 0, lies on the hodograph $R(\varphi)$.

Such a scheme of obtaining the values of $(\mathbf{v} \cdot \mathbf{H})$ is shown in Fig. 1: the straight line $DF \perp \mathbf{H}$ is tangent to the contour $R(\varphi)$. It is seen that the values of $(\mathbf{vH})_{\max}$ and $\mathbf{v}_{\lim}(\mathbf{H})$ are identical only in the directions of the principle axes of the ellipse and in the general case they cannot differ by more than severalfold [for a given $\mathbf{H}$ this ratio depends, of course, on the anisotropy α of the ellipse (1)]. It is also seen that the dependence $v_{\lim}(\varphi)$ is much more anisotropic than the dependence $M(\varphi)$, although their maximal and minimal values are identical.

For the ellipse, it is not difficult to show that the value $(\mathbf{v} \cdot \mathbf{H})_{\max}$ is realized at the point C where the corresponding ray $\mathbf{H}$, drawn from the origin, intersects the contour (1). Actually, solving the problem of the conditional extremum of the function

$$\psi = \Phi + \mu(ak_x^2 + bk_y^2), \tag{6}$$

where $\Phi = (\mathbf{v} \cdot \mathbf{H})$ is the functional whose maximum is sought and μ is a Lagrange multiplier, we obtain

$$\nabla\psi = \nabla(\mathbf{vH}) + \mu\mathbf{v} = 0. \tag{7}$$

From (7), we obtain the extremum condition

$$2\begin{pmatrix} a & H_x \\ b & H_y \end{pmatrix} + 2\mu\begin{pmatrix} a & k_x \\ b & k_y \end{pmatrix} = 0, \quad \text{i.e.,} \quad \frac{k_y}{k_x} = \frac{H_y}{H_x}. \tag{8}$$

We obtain the equation for the function $M(\varphi)$. We write down (see the notation in Fig. 1 near the point C): $M(\varphi) = v(\varphi)\cos\alpha = v(\varphi)\sin\omega$, for the angle α we have $\operatorname{tg}\omega = k(\varphi)/k'(\varphi)$, where $k(\varphi)$ and $v(\varphi)$ are determined from (2) and (3). After a number of transformations, we obtain

$$M(\varphi) = 2E_0^{1/2}(a\cos^2\varphi + b\sin^2\varphi)^{1/2}. \tag{9}$$

We can show that the dependence (9) at $\alpha > \alpha_{cr}^{(M)}$, where

$$\alpha_{cr}^{(M)} = 2^{1/2}, \tag{10}$$

has "wings," just as $v = v(\varphi)$.

For the dependence of the ratio $A(\varphi) \equiv M(\varphi)/v_{\lim}(\varphi)$ on φ, we obtain

$$A(\varphi) = {}^1/_2 (ab)^{-1/2}[(b-a)^2 \sin 2\varphi + 4ab]^{1/2}. \tag{11}$$

It follows from (11) that the value of $A(\varphi)$ is a maximum at $\varphi = \pi/4$:

$$A(\varphi)_{max} = A(\pi/4) = {}^1/_2 (ab)^{-1/2}(a+b). \tag{12}$$

It is clear that for any anisotropy $\alpha (\alpha \neq 1) A(\varphi) > 1 (\varphi \neq \pi n/2)$.

It is entirely evident that operations analogous to (6)–(8) lead to a conclusion identical to (8) for any ellipsoidal equal-energy surface, i.e., in the case

$$ak_x^2 + bk_y^2 + ck_z^2 = E_0 \tag{13}$$

the maximum value of the functional $\Phi = (\mathbf{v} \cdot \mathbf{H})$ for a given direction of $\mathbf{H}$ is realized at the point of the ellipsoid at which the ray of this direction "pricks" the surface, i.e., at that point of the ellipsoid, which satisfies the relation

$$k_x/H_x = k_y/H_y = k_z/H_z. \tag{14}$$

It is easy to grasp that the hodograph of the Fermi velocities for (13) will [in analogy with (5)] be the ellipsoid[2)]

$$k_x^2/a + k_y^2/b + k_z^2/c = 4E_0. \tag{15}$$

The surface characterizing the distribution $(\mathbf{v} \cdot \mathbf{H})_{\max}$ will encompass the ellipsoid (15) and be tangent to it at points lying on its principal axes.

For the determination of $M(\varphi)$ and $v_{\lim}(\varphi)$ in the case of real Fermi surfaces, special calculation procedures were developed.

3. SCHEME OF CALCULATIONS OF "VELOCITY" CHARACTERISTICS

We first consider the general setup of the problem. We need to find on the Fermi surface the point $\mathbf{k}^*$ that makes stationary the given functional $\Phi(\mathbf{k},\mathbf{H})$, where $\mathbf{H}$ is a certain unit vector serving as a parameter, and stipulate the determination of a set of points $\{\mathbf{k}^*(\mathbf{H})\}$, when $\mathbf{H}$ takes on all possible directions in some plane.

The procedure of the determination of the point $\mathbf{k}^*$ was set up according to an "adaptive-gradient" scheme. This means that the vectors $\mathbf{v}_0$ and $\nabla\Phi(\mathbf{k}_0) \equiv \Phi_0$ are calculated at some initial point $\mathbf{k}_0$ on the Fermi surface. The direction of

motion in the $(n+1)$st step was determined by the direction of the projection of $\mathbf{\Phi}_m$ in the plane tangent to the Fermi surface. The corresponding unit vector $\mathbf{l}_{m+1}$ is obviously equal to

$$\mathbf{l}_{n+1}=\mathbf{L}_{n+1}/L_{n+1}, \tag{16}$$

where

$$\mathbf{L}_{n+1}=\mathbf{\Phi}_n-\mathbf{v}_n(\mathbf{v}_n\mathbf{\Phi}_n)/v_n^2.$$

The magnitude of the displacement Δ_{n+1} in the direction of $\mathbf{l}_m$ is not connected with $\mathbf{\Phi}_n$, but depends exclusively on the magnitude of the displacement Δ_m calculated in the previous step, and on the value of the function $\mathrm{Sg}(\Phi_n-\Phi_{n-1})$, which is equal to $\mathrm{Sg}=0$ if the nth step brings Φ closer to a stationary value, and $\mathrm{Sg}=1$ if it moves it further away:

$$\Delta_{n+1}=\Delta_n(1-0.5\mathrm{Sg}); \tag{17}$$

here the value of Δ_0 was specified in the adjustment procedure (usually $\Delta_0\sim 0.01$).

The relations (16) and (17) lead to the following formula for calculation of the point $\mathbf{k}_{m+1}$:

$$\mathbf{k}_{n+1}=\mathbf{k}_n+\mathbf{l}_{n+1}\Delta_{n+1}. \tag{18}$$

The following three functions enter into the problems that we have considered (the third is auxiliary):

a) $\Phi^{(1)}=\mathbf{vH}$, so that

$$\Phi^{(1)}=\|\hat{E}\|\mathbf{H}, \quad \mathbf{L}^{(1)}=\|\hat{E}\|\mathbf{H}-\mathbf{v}(\mathbf{v}\|\hat{E}\|\mathbf{H})/v^2; \tag{19a}$$

b) $\Phi^{(2)}=(\mathbf{vH})/v$, so that

$$\Phi^{(2)}=\|\hat{E}\|\mathbf{z}/v, \quad \mathbf{L}^{(2)}=\|\hat{E}\|\mathbf{z}-\mathbf{v}(\mathbf{v}\|\hat{E}\|\mathbf{z})/v^2; \tag{19b}$$

where $\mathbf{z}=\mathbf{H}-\mathbf{v}(\mathbf{vH})/v^2$;

c) $\Phi^{(3)}=(\mathbf{kH})$, so that

$$\Phi^{(3)}=\mathbf{H}, \quad \mathbf{L}^{(3)}=\mathbf{H}-\mathbf{v}(\mathbf{vH})/v^2=\mathbf{z}. \tag{19c}$$

The third functional is obviously the projection of the radius vector $\mathbf{k}$ of the Fermi surface on the direction $\mathbf{H}$; its maximum is achieved at the limiting (for a given $\mathbf{H}$) point $\mathbf{k}_m$ that coincides with the reference point. Therefore, the problem of the extremalization of the functional $\Phi^{(2)}$ for most of our problems (more precisely, for convex surfaces) was reduced to the simpler problem of the extremalization of the functional $\Phi^{(3)}$. This is seen also from the relations (21b) and (21c): the equality $z=0$ is the general condition of termination of the iterative processes connected with the extremalization of these functionals.

We shall now give some more specifics about the search for the points $\mathbf{k}^*(\varphi)$. The calculation of the value of $(\mathbf{v}\cdot\mathbf{H})_{\max}$ was begun with finding the point $\mathbf{k}_0$ belonging to the Fermi surface and lying on the given ray $\mathbf{H}$. The point $\mathbf{k}^*$ that guarantees the maximum of the functional $\Phi_{k\in FS}=(\mathbf{v}\cdot\mathbf{H})$ was always not far from $\mathbf{k}_0$ and was found by the method of succesive approximations with the use of (18) and (19a).

The calculation of $\mathbf{v}_{\mathrm{lim}}(\mathbf{H})$ turns out to be a more cumbersome problem. In this case, each step of the iteration consists of two steps:

a) the transition from the point $\mathbf{k}_{n-1}$ to the point $\mathbf{k}_m$ according to (18), in which the unit vector $\mathbf{l}_m$ was determined from (19c) or, in case of necessity, from (19b);

b) return of the variable point $\mathbf{k}$ to the Fermi surface. Since the limiting point of the Fermi surface is located, as a rule, far from the initial point $\mathbf{k}_0$, the point $\mathbf{k}_m$ can be significantly far removed from the Fermi surface (i.e., the difference $E(\mathbf{k}_m)-E_F=\varepsilon_m$ can exceed the error of calculation of $E(\mathbf{k})$, which is equal to 0.0001 atomic units in our calculations); in this case, using the approximation $\varepsilon(\mathbf{k})\approx\varepsilon_n+(\mathbf{k}-\mathbf{k}_n)\mathbf{v}_n$, we "drew" the variable point to the Fermi surface, i.e., the second step was reduced to the transition

$$\mathbf{k}_{n+1}=\mathbf{k}_n-\mathbf{v}_n\varepsilon_n/v_n^2. \tag{20}$$

Having found the point $\mathbf{k}_{m+1}$, we calculate $\mathbf{v}_{m+1}$ and ε_{m+1}. If $|\varepsilon_{n+1}|\leqslant 0{,}0001$, then we proceed to the completion of step a) for the next stage of the procedure; in the opposite case, we again turn to the relation (20).

4. FERMI VELOCITIES IN Sb AND Bi; COMPARISON WITH EXPERIMENT

In the numerical calculations, it is important to secure convergence of the results in dependence on the dimensionality of the secular matrix. Careful investigations of the dependences of the calculated values of the velocity components v_i in Sb on the dimensionality of the secular matrix M, carried out by us, have shown that at $M=90$ the calculated error in the computation of the Fermi velocities of both electrons and holes amounted to several percent. Further reduction in the calculated error does not make sense, because the results given below for Sb were obtained at $M=90$

Figure 2 shows the following: the "hedgehog" for the

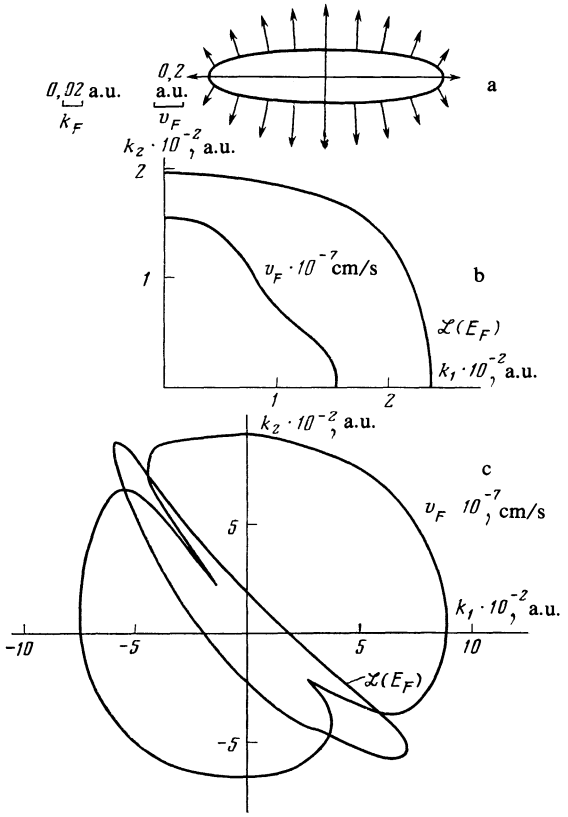

FIG. 2. Contours of the sections of the Fermi surface of Sb: $S^e_{\max}$ (a), $S^e_{\min}$ (b) and S^e_{bin} (c) together with the distribution of velocities $v(\varphi)$; the scale of v for b and c follows from the text.

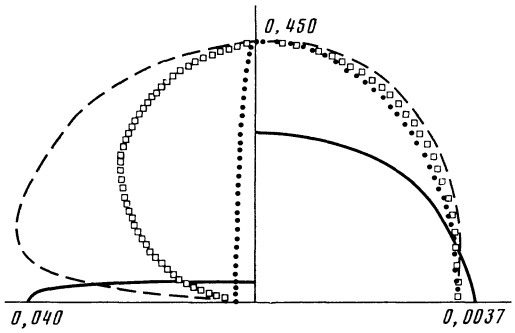

FIG. 3. Polar diagrams $v(\varphi)$, $M(\varphi)$, and $V_{\lim}(\varphi)$ together with the contours of the sections of the Fermi surface (Bi) for $S^e_{\min}$ (at the right) and $S^e_{\max}$ (at the left). The notation is the same as that of Fig. 1. The scale for v_F is shown on the ordinate, the scale for k_F (which is different for $S_{\min}$ and $S_{\max}$) on the abscissa.

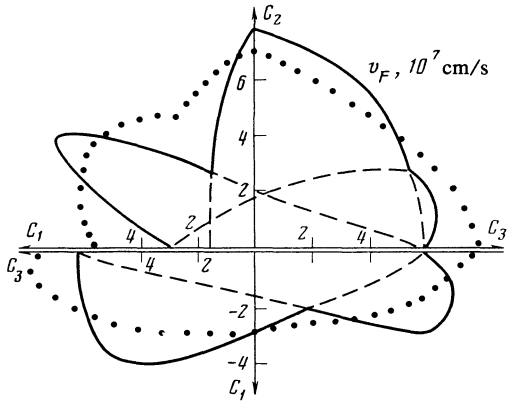

FIG. 4. Polar diagrams of $v_{\lim}(\varphi)$ for electrons in Sb in the three crystallographic axes. The points are from the experiments of Ref. 11, the solid curve is a calculation, the dashed curve is formed by pieces of the polar diagrams of individual electron "pockets" of the Fermi surface.

section $S^e_{\max}$ and the polar diagrams of $v(\varphi)$ for $S^e_{\min}$ and $S^h_{\min}$ in Sb. Attention should be paid to the dependence $v = v(\varphi)$ along the contour of the section $S^e_{\min}$. According to (3), $v = v(\varphi)$ is a monotonic function, but calculation leads to a nonmonotonic dependence $v = v(\varphi)$ with an absolute by minimal (for this cross section) value of the velocity $v^{(\text{abs})}_{\min} = 6{,}21 \cdot 10^7$ cm/s. Such a result of the calculation may seem surprising, but it is not difficult to verify that it correlates excellently with the fact (previously obtained by us in Ref. 7) that the shape of $S^e_{\min}$ changes under pressure.

Polar diagrams of $v(\varphi)$ and $M(\varphi)$ are shown in Fig. 3, as well as hodographs of the Fermi surfaces and the contours of the sections of the Fermi surface of Bi for $S^e_{\max}$ and $S^e_{\min}$, calculated from the spectrum of McClure and Choi.[9] The anisotropies of the section $S^e_{\max}$ lead to a value of α which is a little larger than α_{cr} from (4) and (10); therefore, the appearance of "wings" and "funnels" for $v(\varphi)$ and $M(\varphi)$ is not surprising. But, if we compare the details of $v(\varphi)$, $M(\varphi)$ and $A(\varphi)$ for this section with the relations (3), (9) and (11), then the effect of the deviation of the electron spectrum of the model of Ref. 9 from the simple ellipsoidal model is noticeable. Thus, for example, for the value $A(\pi/4)$ we have 6.0, while according to (12) we would obtain 1.9 (for $S^e_{\min}$ the corresponding values are 1.04 and 1.01).

The most complete comparison with experiment can be carried out by using the data of Ref. 11 on the measurement of the tilt effect with Sb and Bi, which consists in a strong increase in the second absorption when the magnetic field vector H is tilted to a small angle from the direction $\mathbf{H} \perp \mathbf{q}$ ($\mathbf{q}$ is the wave vector of the sound wave). According to Ref. 2, this effect is due to the absorption of sound by electrons from the vicinity of the elliptical limiting point, and it allows us to determine the velocity of the electrons at this point. To be precise, at a certain critical tilt angle φ_{cr},

$$\varphi_{cr} = \arcsin(s/v_{\lim}(\mathbf{H})) \tag{21}$$

(s is the sound velocity), a group of charge carriers appears from the vicinity of the limiting point of the Fermi surface, moving in phase with the wave and effectively absorbing the sound-wave energy.

As was shown in Ref. 3, at $\omega\tau \gg 1$ (ω is the sound frequency, τ is the relaxation time), the angular position φ_0 of the point of inflection on the curve of the dependence of the absorption coefficient Γ on the tilt angle, $\Gamma = \Gamma(\varphi)$, is identical, with great accuracy, with the value φ_{cr}. In recording the derivative Γ'_φ the points of inflection are determined as the spikes (extrema) on the curve. Experiments[11] and estimates carried out by the authors on the oscillations of the geometric resonance and the shape of the curve $\Gamma(\varphi)$ yielded $\omega\tau = 1.5$. Numerical calculation according to the formulas from Ref. 3 shows that this leads to a lowering of the measured velocities by 15%. In the case, however, in which the $\Gamma(\varphi)$ dependence is a superposition of contributions from several regions, the authors of Ref. 11 were unable to introduce a similar correction.

Measurement of the angles φ_0 has been carried out in Ref. 11 at three orientations relative to the crystallographic axes: $\mathbf{q} \| X (\| C_2)$-here, the projections of the Fermi velocity on the trigonal-bisecting plane C_1C_3 is determined; C_1C_3; $\mathbf{q} \| Y (\| C_1)$ gives the projection of $\mathbf{v}_F$ on the trigonal-binary plane C_2C_3: $\mathbf{q} \| Z (\| C_3)$ gives the projection of $\mathbf{v}_F$ on the binary-bisecting plane C_1C_2.

The polar diagrams $v_{\lim}(\varphi)$ are shown in Fig. 4 for Sb in the three crystallographic plane C_1C_2, C_2C_3 and C_1C_3, obtained in the experiments of Ref. 11, and also calculated by us, and the values of v_F for a number of specific crystallographic directions, are tabulated in Table I. Experimental data, obtained in Ref. 12, are also included in this Table, as well as the calculations of Ref. 11 carried out in the quadratic approximation and according to the empirical model of the electron spectrum of Sb constructed from experimental data on the basis of the Lifshitz-Pogorelov[13] theory by the procedure suggestd by Mueller.[14]

Fair agreement of our calculated values with the experimental data is seen from Fig. 4 and Table I, and it must be taken into account that the experimental values of Fig. 4 and Table I are given without correction for the finiteness of $\omega\tau$. The greatest difference is observed in the directions of $(v_{\lim})_{\min}$ in the C_1C_2 plane, where $v_F^{\text{exp}}/v_F^{\text{calc}} \approx 2$ We defer the discussion of these differences to Sec. 5.

Polar diagrams of $v_{\lim}(\varphi)$ for Bi in the three crystallographic planes C_1C_2, C_2C_3 and C_1C_3 are shown in Fig. 5.

TABLE I. Fermi velocities (in 10^7 cm/s) for a number of crystallographic directions in Sb.

Source	Electrons				Holes
	v_x	v_y	v_z	v *	v **
Experiment [11]	6,80	2,70	7,90	7,55	10,5
Experiment [12]	–	–	–	7,10	11,66
Our calculation	7,61	2,80	6,17	7,52	9,1
Empirical model [11]	6,20	3,71	8,80	7,18	–
Quadratic approximation [11]	6,54	2,50	5,26	5,20	9,72

*The direction makes an angle of 5° with the C_3 axis in the ZY plane.
**The direction makes an angle of 35° with the C_3 axis in the ZY plane.

These were obtained experimentally and also calculated by us. Figure 5 also shows the values of the velocities with correction for the finiteness of the quantity $\omega\tau$. This correction significantly improved the agreement between calculation and experiment in those directions where the contribution to the effect of the charge carriers from a single region of the Fermi surface predominates heavily. As has already been noted,in the more complicated cases of the superposition of contributions of different regions of the Fermi surface, a similar correction of the experimental values of v_F becomes difficult.

In Table II are given the experimental values, and those calculated by us, of the velocities of the electrons in Bi in the directions of the principal axes of the electronic "ellipsoid."

As a whole, good agreement of experiment and theory must be acknowledged. The greatest divergence, as in the case of Sb, is observed in the direction of $(v_{\text{lim}})_{\min}$ in the C_1C_2 plane, where $v_F^{\text{exp}}/v_F^{\text{calc}} \sim 2$.

5. CONCLUSIONS AND DISCUSSION

We have demonstrated the possibility of calculating the "velocity" characteristics of the Fermi surface both in the scheme of a pseudopotential and also outside of this scheme. We have given examples of calculated "hedgehogs" and pictures with "halos" for certain plane sections of the electron and hole parts of the Fermi surface of Sb.

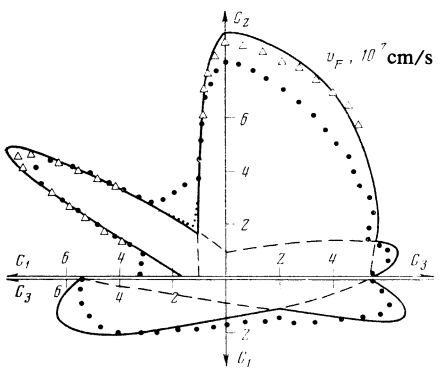

FIG. 5. Polar diagrams of $v_{\text{lim}}(\varphi)$ for electrons in Bi in the three crystallographic planes. The basic notation is the same as in Fig. 4. Additional symbols are: △–values of the velocities with correction for the finiteness of $\omega\tau$ (from Ref. 11); in the "funnel" of the diagram in the C_1C_2 plane the small dots are the results of dispersion-law calculations carried out in Ref. 11 in the quadratic approximation.

In addition to the calculation of the values of $\mathbf{v}(\mathbf{k}_F)$ at some point $\mathbf{k}_F$ lying on the Fermi surface, we have shown the method of calculating (with a brief description of the corresponding algorithms) polar diagrams of $v_{\text{lim}}(\varphi)$ and $M(\varphi)$. These characteristics of the Fermi surface of metals (more accurately, the characteristics of the dispersion law $E = E(\mathbf{k})|_{\mathbf{k}=\mathbf{k}_F}$) directly determine a number of observable effects.

The so-called tilt effect was considered from among these effects. Figure 4 and Table I (Sb), and Fig. 4 and Table II (Bi) were devoted to a comparison of the calculations with experiment. At first glance, the comparison of Figs. 4 and 5 (especially in the C_1C_2 planes) suggests better agreement of theory with experiment in the case of Bi than in the case of Sb. But, as we have noted, both in the case of Sb and in the case of Bi the greatest divergence was observed in the C_1C_2 planes in the directions corresponding to $(v_{\text{lim}})_{\min}$, i.e., in the "craters" of the diagrams, while in both cases we have $v_F^{\text{exp}}/v_F^{\text{calc}} \sim 2$ for these directions. Because of the great anisotropy of the electron "ellipsoid" in the case of Bi, this discrepancy extends over a smaller area of the diagram and appears to be visually smaller.

It should therefore be recognized that the measure of agreement between theory and experiment in the cases of Bi and Sb is about the same.

What can be thought of the significant divergence between theory and experiment in the "funnels" of the diagrams in the C_1C_2 planes? It must be remarked that in Refs. 2, 3 and 14 the formula analogous to (21), contains not $\mathbf{v}_{\text{lim}}(\mathbf{H})$ but $(\mathbf{v}\cdot\mathbf{H})_{\max}$ which these authors nevertheless take

TABLE II. Values of v_F (in 10^7 cm/s) of electrons in Bi along the principal axes of the "ellipsoid." (Curve 1–axis of the ellipsoid, axis 3–binary axis)

Source	v_1	v_2	v_3
[10] *	0,89	7,5	10,0
[16] **	–	7,5	9,9
Our calculation	0,83	7,5	9,9

*Calculated from the radii of curvature (see Ref. 10) and the results of measurement of the resonances of the magnetic surface levels in Ref. 15 (for v_1) and Ref. 16 for v_2 and v_3.
**It was also demonstrated in Ref. 16 that the velocities of electrons on the minimal sections of the Fermi surface change according to an elliptical law; this agrees with Fig. 3.

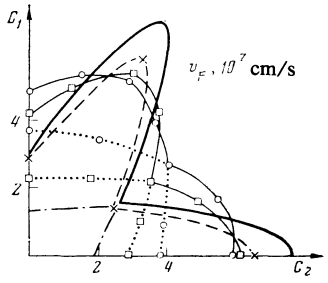

FIG. 6. Corrected polar diagram of $v_{\lim}(\varphi)$ for electrons in Sb in the C_1C_2 plane. The crosses and dashed lines are the experimental data corrected by us according to Table I. The heavy continuous curve is our calculation. The fine continuous lines: with □—the calculation according the quadratic approximation, with ○—the calculation according to the empirical model, (both from Ref. 11). The dotted and dot-dash curves are pieces of the polar diagrams of the individual pockets of the Fermi surface.

to mean the quantity $v_{\lim}(\mathbf{H})$. This is apparently due to the misunderstanding, mentioned in footnote 1), whereby the value $(\mathbf{v}\cdot\mathbf{H})_{\max}$ is seemingly reached at the limiting point of the surface. The values of $(\mathbf{v}\cdot\mathbf{H})_{\max}$ and $\mathbf{v}_{\lim}(\mathbf{H})$ are identical only in the directions of the principal axes of the ellipsoids. For the other directions, $(\mathbf{v}\cdot\mathbf{H})_{\max}\neq\mathbf{v}_{\lim}$, and therefore, generally speaking, the question arises as to the selection of effective electrons. Replacement of the curve $v_{\lim}(\varphi)$ by $M(\varphi)$ significantly raises the bottoms of the calculated "funnels." But the electrons from the region with $(\mathbf{v}\cdot\mathbf{H})_{\max}$ will not be in phase with the sound wave, and therefore their role will obviously not be significant.

We think that the reason for the discussed discrepancy is the incorrect determination in Ref. 11 of the velocity $v_{\lim}(\varphi)$ in the C_1C_2 plane. At the very least, careful analysis of the experimental diagrams of Sb and Bi shown in Ref. 11 (see 4 and 5) reveals significant internal inconsistencies (cf. the value of v_y from the rotation diagrams in the C_1C_2 and C_1C_3 planes). There is significant discrepancy also between the experimental values of v_y in Sb, given in Ref. 11 on the graph and in the table (see Fig. 4 and Table I). If the tabulated experimental value $v_g = 2.7\cdot 10^7$ cm/s, which agrees with the diagram value of v_y in the C_1C_3 plane, is used in the graph, then the calculated and experimental plots of Fig. 4 for the C_1C_2 plane will be close together.

In Fig. 6, we show the experimental diagram, corrected in this fashion, for Sb in the C_1C_2 plane; as well as the rsults of the calculations of Ref. 11 according to the quadratic and empirical models of the electron spectrum of Sb. It is seen that both models describe the experiment worse (if, in analogy with Bi, we take into account the correction for the finiteness of $\omega\tau$ for the regions of predominant contribution from a single electron "pocket," then our calculated result and the corrected experimental dependences are almost equal).

Similarly, if the value of v_y from the diagram in the C_1C_3 is used for Bi, the bottom of the "funnel" from the experimental points in the C_1C_3 plane is lowered and the experimental and calculated diagrams merge. By the same token (as a particular result of the calculations that have been performed), a definite error appears in the representation of the experimental data of Ref. 11. If this error is eliminated, the results of the calculations of the velocities of electrons in Sb and Bi that have been carried out are in good agreement with the entire set of experimental data.

In conclusion, it should be recalled that the electron-phonon correction δv_F is proportional to the area of the Fermi surface (see, for example, Ref. 17) and therefore it should in principle be small in the case of semimetals.

[1)] In spite of a rather widespread opinion, these distributions are entirely different even for ellipsoidal energy surfaces.

[2)] Actually, if the radius vector $\mathbf{k}_0 = \{k_{0x}, k_{0y}, k_{0z}\}$ satisfies (13), then the coordinates of the velocity vector at this point of the surface $\mathbf{v}_0 = \{2ak_{0x}, 2bk_{0y}, 2ck_{0z}\}$ will satisfy Eq. (15).

[1]Yu. A. Pospelov, Fiz. Metal. Metallov. **52**, 455 (1981).
[2]H. Spector, Phys. Rev. **120**, 1261 (1960).
[3]A. P. Korolyuk, M. A. Obolenskii and V. L. Fal'kov, Zh. Eksp. Teor. Fiz. **59**, 377 (1970) [Sov. Phys. JETP **32**, 205 (1971)].
[4]G. P. Ivanovski and M. N. Kaganov, Zh. Eksp. Teor. Fiz. **83**, 2320 (1982) [Sov. Phys. JETP **56**, 1345 (1982)].
[5]L. M. Falicov and P. J. Lin, Phys. Rev. **141**, 562 (1966).
[6]Yu. A. Pospelov, Pis'ma Zh. Eksp. Teor. Fiz. **29**, 215 (1979) [JETP Lett. **29**, 192 (1979)].
[7]Yu. A. Pospelov, Phys. Stat. Solidi (b) **99**, 173 (1980).
[8]Yu. A. Pospelov and G. S. Grachev, J. Phys. F: Met. Phys. **13**, 1179 (1983).
[9]J. W. McClure and K. H. Choi, Sol. State Comm. **21**, 1015 (1977).
[10]V. S. Edel'man, Usp. Fiz. Nauk **123**, 257 (1977) [Sov. Phys. Uspekhi 20, **819** (1977)].
[11]V. I. Beletskiĭ, A. V. Golin, A. P. Korolyuk and M. A. Obolenskiĭ, Zh. Eksp. Teor. Fiz. **69**, 1045 (1975) [Sov. Phys. JETP **42**, 531 (1975).
[12]H. Suematsu, N. Koshino and S. Tanuma, J. Low. Temp. Phys. **15**, 281 (1974).
[13]I. M. Lifshitz and A. V. Pogorelov, Dokl. Akad. Nauk SSSR **96**, 1143 (1954).
[14]F. M. Mueller, Phys. Rev. **148**, 636 (1966).
[15]S. Takaoka, H. Kawamura, K. Murase and S. Takano, Phys. Rev. B **13**, 1428 (1976).
[16]J. F. Koch and J. D. Jensen, Phys. Rev. **184**, 643 (1969).
[17]M. I. Kaganov and T. Yu. Lisovskaya, Zh. Eksp. Teor. Fiz. **80**, 2445 (1981) [Sov. Phys. JETP **53**, 1280 (1981)].

Translated by R. T. Beyer